Title

Topological edge conduction induced by strong anisotropic exchange interactions

Journal

Physical Review B, 110(10)

ISSN

2469-9950

Authors

Sayed, Shehrin

Brahma, Pratik

Hsu, Cheng-Hsiang

et al.

Publication Date

2024-09-01

DOI

10.1103/physrevb.110.l100407

Topological edge conduction induced by strong anisotropic exchange interactions

Shehrin Sayed,[1,2,3,*] Pratik Brahma,[2] Cheng-Hsiang Hsu,[2] and Sayeef Salahuddin[1,2,†]
[1]*Materials Sciences Division, Lawrence Berkeley National Laboratory, Berkeley, California 94720, USA*
[2]*Electrical Engineering and Computer Sciences, University of California, Berkeley, California 94720, USA*
[3]*TDK Headway Technologies, Inc., Milpitas, California 95035, USA*

We predict that an interplay between isotropic and anisotropic exchange interactions in a honeycomb lattice structure can lead to topological edge conduction when the anisotropic interaction is at least twice the strength of the isotropic interaction. For materials like Na_2IrO_3, such a strong anisotropic exchange interaction simultaneously induces a zigzag type of antiferromagnetic order that breaks the time-reversal symmetry of the topological edge conductor. We show that the electronic transport in such topological conductors will exhibit a quantized Hall conductance without any external magnetic field when the Fermi energy lies within a particular energy range.

Recently, there is a growing interest in transition metal-based oxides and halides with honeycomb lattice structure [1–3] [see Fig. 1(a)] for exhibiting both isotropic and bond-dependent anisotropic exchange interactions [4]. An interplay between these exchange interactions can lead to quantum magnetism [5–11] and a spin liquid state [11–14], which are modeled using the Kitaev-Heisenberg (KH) model as given by

$$\mathcal{H} = \sum K^{\gamma} S_i^{\gamma} S_j^{\gamma} + \sum J \vec{S}_i \cdot \vec{S}_j, \tag{1}$$

where $\gamma \equiv \{x, y, z\}$, K^{γ} is the anisotropic exchange interaction along the γ bond, J is the isotropic exchange interaction, and $\vec{S}_i = \sum_{\gamma \equiv \{x,y,z\}} \hat{\gamma}\, S_i^{\gamma}$ is the spin-$\frac{1}{2}$ operator on the ith lattice point.

In this Letter, we predict that an interplay between the isotropic and anisotropic exchange interactions can form topological edge states when the anisotropic exchange interaction is at least twice the strength of the isotropic exchange interaction. Such an interplay will simultaneously induce an intrinsic magnetic order, specifically a zigzag antiferromagnetic (AFM) order, that breaks the time-reversal symmetry (TRS) of the edge conductor. We use a tight-binding model for such materials [15–17], and a nonequilibrium Green's function (NEGF)-based quantum-transport model [18] to show that the exchange interaction induced topological edge conduction will exhibit a Hall conductance quantized to q^2/h (where q is the electron charge and h is the Planck's constant) when the current is running along the zigzag direction and the voltage is measured along the armchair direction. We further calculate the band structures and Hall conductances of Na_2IrO_3 and α-$RuCl_3$, and show that Na_2IrO_3 could be a model material to observe the phenomena predicted in this Letter. Finally, using one-dimensional approximations and analytical arguments, we show that the topological edge state formation for high anisotropic exchange interaction is a property of Eq. (1).

Transition-metal-based oxides and halides with honeycomb lattice structures have a half-filled d^5 ion (e.g., Ir^{4+} or Ru^{3+}) in each of the lattice points in an octahedral environment. The crystal field (CF) splits the d orbital into a e_g (equally degenerate) pair and t_{2g} (triply degenerate) states, see Fig. 1(a), and all five electrons occupy the t_{2g} states. The presence of spin-orbit coupling (SOC) further splits the t_{2g} states into $j_{\text{eff}} = \frac{1}{2}$ and $\frac{3}{2}$ states [see Fig. 1(a)], where the $j_{\text{eff}} = \frac{3}{2}$ states are filled and the $j_{\text{eff}} = \frac{1}{2}$ state is half-filled. Thus, we have one hole per site. We describe the hole-mediated transport in such materials using a tight-binding Hamiltonian, given by

$$\mathcal{H} = H_U + H_{\text{CF}} + H_{\text{SOC}} + H_{\text{hop}}, \tag{2}$$

which is in the basis of the d_{xy}, d_{yz}, and d_{zx} orbitals with each orbital having two spin states, i.e., $\Psi \equiv \{\psi_{xy}^{\uparrow}, \psi_{xy}^{\downarrow}, \psi_{yz}^{\uparrow}, \psi_{yz}^{\downarrow}, \psi_{zx}^{\uparrow}, \psi_{zx}^{\downarrow}\}$. Equation (2) takes into account the static inter and intraorbital Coulomb repulsion (H_U), crystal field (H_{CF}), spin-orbit coupling (H_{SOC}), and hole-based hopping ($H_{\text{hop.}}$) with bond-dependent hopping integrals (t_1 to t_{10}) shown in Fig. 1(b) [19]. The effective values of the hopping integrals are adopted from Ref. [15], which were obtained by fitting detailed DFT calculations considering electron-electron interactions.

The isotropic (J) and anisotropic ($K^z = K^x = K^y = K$) exchange interaction strengths in Eq. (1) are related to these hopping integrals as [15–17]

$$J = \delta\,(2t_1 + t_3)^2 - \xi\left\{9t_4^2 + 2(t_1 - t_3)^2\right\}, \tag{3a}$$

$$K = \xi\left\{3t_4^2 + (t_1 - t_3)^2 - 3t_2^2\right\}, \tag{3b}$$

where the coefficients δ and ξ are determined by the Coulomb repulsion, Hund's coupling, and SOC strengths [15–17]. We have solved Eq. (1) in Fock space to find the ground energy

*Contact author: shehrin.sayed@tdk.com
†Contact author: sayeef@berkeley.edu

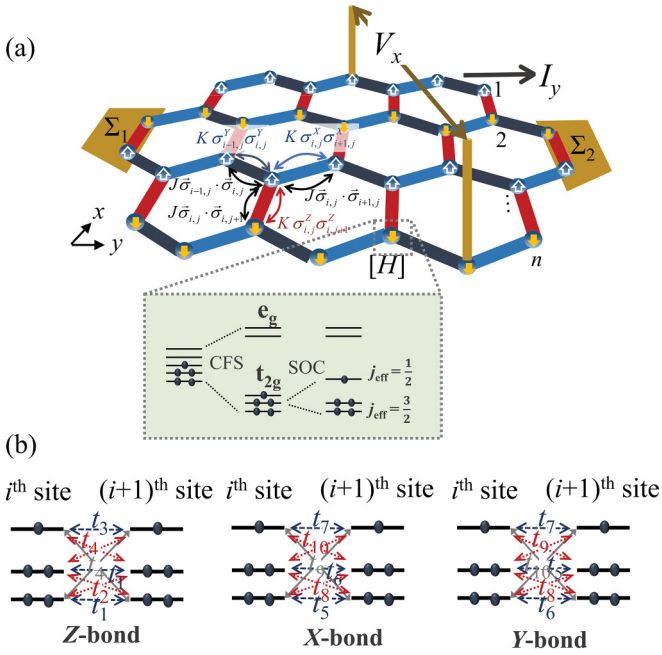

FIG. 1. (a) A honeycomb lattice with isotropic (J) and bond-dependent anisotropic (K) exchange interactions. Local d-orbital states on each lattice point in the presence of Coulomb interaction (U), crystal field splitting (CFS), and spin-orbit coupling (SOC). (b) General nearest neighbor hopping scenario along different bonds.

state and corresponding intrinsic magnetic order for a particular combination of J and K calculated using the tight-binding parameters for Na_2IrO_3 [15].

We use the tight-binding model in Eq. (2) to calculate the Green's function $\mathcal{G} = [E\mathcal{I} - \mathcal{H} - \Sigma_0 - \Sigma_1 - \Sigma_2]^{-1}$ for the structure in Fig. 1(a), where E is the energy, $\mathcal{I}$ is the identity matrix, $\Sigma_{1,2}$ are the self-energy functions of the left and right contacts, respectively, and $\Sigma_0 = \mathcal{W}\mathcal{G}$ is the self-energy that takes into account the dephasing in the channel due to electron-electron interactions in a self-consistent manner. Here $\mathcal{W}_{m,n} = \langle U_m U_n^* \rangle$ is calculated from the random potential at mth and nth lattices. We use Green's function [18,19] to calculate the potential distribution on the xy plane as

$$V(x,y) = V_0 \,\mathrm{Re}\left\{\frac{\mathcal{G}(\Gamma_1 f_1 + \Gamma_2 f_2)\mathcal{G}^\dagger}{\mathcal{G}\,(\Gamma_1+\Gamma_2)\mathcal{G}^\dagger}\right\}, \tag{4}$$

where $\Gamma_{1,2} = j(\Sigma_{1,2} - \Sigma_{1,2}^\dagger)$ are the broadening functions and represent the anti-Hermitian parts of the self-energy functions, $f_{1,2}$ are the Fermi occupation factors of the left and right contacts, respectively, and V_0 is the applied potential. The Hall resistance is given by

$$R_{xy} = \frac{\Delta V_x}{I_y} = \frac{V(x=0,y) - V(x=w,y)}{\frac{q}{h}\;dE\;\mathrm{Trace}[\mathrm{Re}\{\Gamma_1\mathcal{G}\Gamma_2\mathcal{G}^\dagger\}]\,(f_1-f_2)}, \tag{5}$$

where the numerator represents the voltage difference between the two zigzag edges along the armchair direction and the denominator represents the current I_y flowing along the zigzag direction. Here, w is the channel width. The Hall conductance G_{xy} is calculated using R_{xy} and longitudinal resistance R_{xx} as $G_{xy} = R_{xy}/(R_{xy}^2 + R_{xx}^2)$.

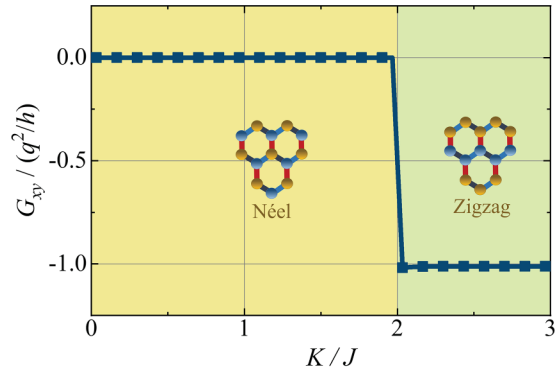

FIG. 2. The Hall conductance (G_{xy}) and corresponding magnetic order as a function of K/J.

In order to understand the effect of the intrinsic exchange interactions in the transport properties, we calculate G_{xy} and the magnetic order of the honeycomb lattice as a function of the relative strength between the anisotropic and isotropic exchange interactions (i.e., $|K/J|$), as shown in Fig. 2. We apply a current I_y along the zigzag chains (y direction) and calculate the transverse voltage V_x along the armchair direction (x direction), see Fig. 1(a). We change the $|K|/|J|$ ratio by changing the hopping integral t_4 and keep other parameters equivalent to the parameter values for Na_2IrO_3. The NEGF calculations show that $|G_{xy}|$ is 0 when $K < 2J$, however, becomes exactly q^2/h when the $K \geqslant 2J$, see Fig. 2. This phenomenon induced by a strong anisotropic exchange interaction in a two-dimensional (2D) channel is very similar to the popular signature of a quantum anomalous Hall (QAH) state [20–23] observed in band-inverted three-dimensional magnetic topological insulators with broken TRS.

The quantized Hall conductance in Fig. 2 is a combination of two effects: topological edge state formation when $K \geqslant 2J$ and intrinsic magnetic ordering induced by the interplay between J and K that simultaneously breaks the TRS. In order to understand the edge state formation, we calculate the local density of states as

$$\mathcal{D} = \frac{1}{2\pi}\mathrm{Re}(\mathcal{G}\,\Gamma\,\mathcal{G}^\dagger), \tag{6}$$

where $\Gamma = j\{\Sigma_1 + \Sigma_2 - (\Sigma_1 + \Sigma_2)^\dagger\}$ is the broadening function. The spatial distribution of the local density of states is shown in Figs. 3(a) and 3(b) for tight-binding parameters that correspond to $K < 2J$ and $K > 2J$, respectively. The density of states is nonzero everywhere throughout the 2D channel when $K < 2J$ and there are no distinct edge states, as shown in Fig. 3(a) for the case $|K|/|J| \approx 0.1$. For $K > 2J$, the density of states in the middle of the 2D channel becomes zero, i.e., the middle of the 2D channel becomes insulating. However, the case of $K > 2J$ exhibits edge states as shown in Fig. 3(b) for $|K|/|J| \approx 2.5$.

To analyze the magnetic order in the honeycomb lattice considered here, we reduce Eq. (1) to a minimal model [15] as given by

$$H = \sum_{\text{1st nn}} J\vec{S}_i \cdot \vec{S}_j + KS_i^\gamma S_j^\gamma \;+ \sum_{\text{3rd nn}} J'\vec{S}_i \cdot \vec{S}_j, \tag{7}$$

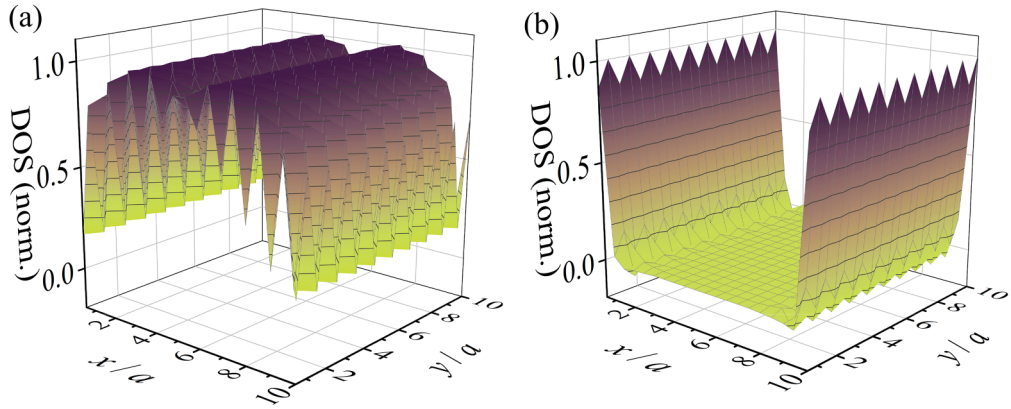

FIG. 3. Local density of states on the two-dimensional honeycomb lattice structure in Fig. 1(a) for (a) $K = 0.1J$ and (b) $K = 2.5J$.

where J and K are the first nearest neighbor Heisenberg and Kitaev interaction coefficients, respectively, and J' is the third nearest neighbor Heisenberg interaction coefficient (see Fig. 4). We solve a 13-spin lattice system in a honeycomb structure containing three hexagons, as shown in Fig. 4. The ground state of the spin-lattice is obtained by sweeping the Hamiltonian parameter K/J from zero to four and exactly diagonalizing. We use the nominal values $(J', K) \sim (0.4, -1)$ meV typically used for Na_2IrO_3 [15] and tune the J parameter for the K/J sweep. The ground-state solution is reasonably robust for the system size under consideration and in agreement with the previously reported results for Na_2IrO_3 [15].

The honeycomb lattice considered here has a Néel type AFM order for $K < 2J$. Thus, the two-dimensional channel in the honeycomb lattice structure does not have an effective field that can produce an anomalous Hall effect and does not contribute to G_{xy}. Thus, we observe $G_{xy} = 0$. However, there is a sharp transition from Néel type AFM order to a zigzag type AFM order for $K > 2J$, see Fig. 2. A zigzag AFM order refers to the case where each of the zigzag atomic chains is a one-dimensional (1D) ferromagnetic chain; however, the ferromagnetic order alternates along the armchair direction [see Fig. 1(a)], giving rise to an overall AFM order. Thus, the edge atomic chains have a net magnetic order that breaks the TRS of the edge conductor. Note that the magnetic order for the case $K = 2J$ is a superposition of a Néel and zigzag AFM states.

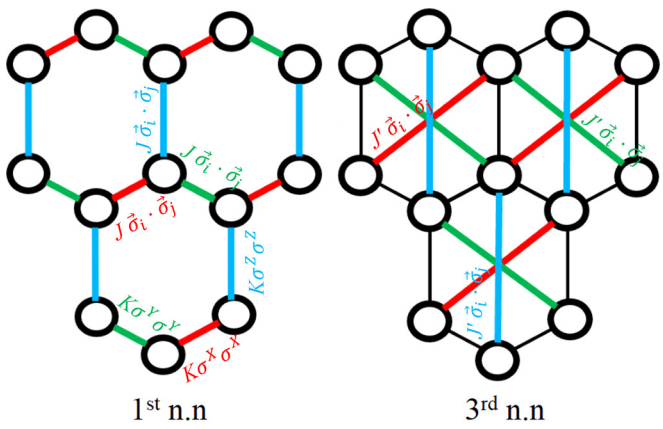

FIG. 4. Visual representation of all first and third nearest-neighbor (n.n) interactions.

Such systems may exhibit mixed-spin interaction terms arising from a pseudodipolar or Dzyaloshinskii-Moriya interaction [15,20,24]. However, magnetic phases in Na_2IrO_3 and α-$RuCl_3$ can be described by a minimal model [15] consisting only of isotropic Heisenberg and anisotropic Kitaev terms up to the third nearest neighbor. Although, the magnetic order was calculated using a minimal model in Eq. (7), the transport calculations considered a general hopping among the t_{2g} states. We leave the study of such mixed-spin-interaction-induced magnetic order on the topological states for the future.

The zigzag AFM order has been observed in the transition metal oxides and halides, e.g., Na_2IrO_3 and α-$RuCl_3$, at low temperatures [5,6,8,9–11]. We calculate the band diagram of Na_2IrO_3 and α-$RuCl_3$ using Eq. (2), see Figs. 5(a) and 5(b), where the tight-binding parameters correspond to a zigzag AFM order. We observe the spin bands for the $j_{\text{eff}} = \frac{1}{2}$ energy states show a small gap of $\sim$26 meV near the M symmetry point for both materials. We have calculated R_{xy} using Eq. (5) as a function of energy within the energy gap and found it to be quantized to h/q^2 for Na_2IrO_3, as shown in Fig. 5(c). This indicates that the energy gap hosts nontrivial topological edge states. Interestingly, the calculated $J \approx 3.4$ meV and $K \approx -22.3$ meV yields $|K|/|J| \approx 6.6$ that satisfies the condition in Fig. 2. This phenomenon will be observed in Hall measurements on Na_2IrO_3 at low temperatures where zigzag AFM forms and as long as the Fermi energy lies within the topological energy gap.

For α-$RuCl_3$, we do not observe a quantized R_{xy} in the transport calculation within the energy gap, see Fig. 5(d). This is consistent with the condition in Fig. 2, as J and K are -2.02 meV and -3.4 meV based on the tight-binding parameters, respectively, which gives $|K|/|J| \sim 1.68$. A nonzero R_{xy} for a small energy range within the upper band is observed, which corresponds to the anomalous Hall effect due to an uncompensated net magnetization in the lattice with a zigzag AFM order. Note that a half-integer quantized Hall effect has been observed for thermal transport [25,26] in α-$RuCl_3$, which is out of the scope of this Letter. In this Letter, we predict an anisotropic exchange interaction induced quantized

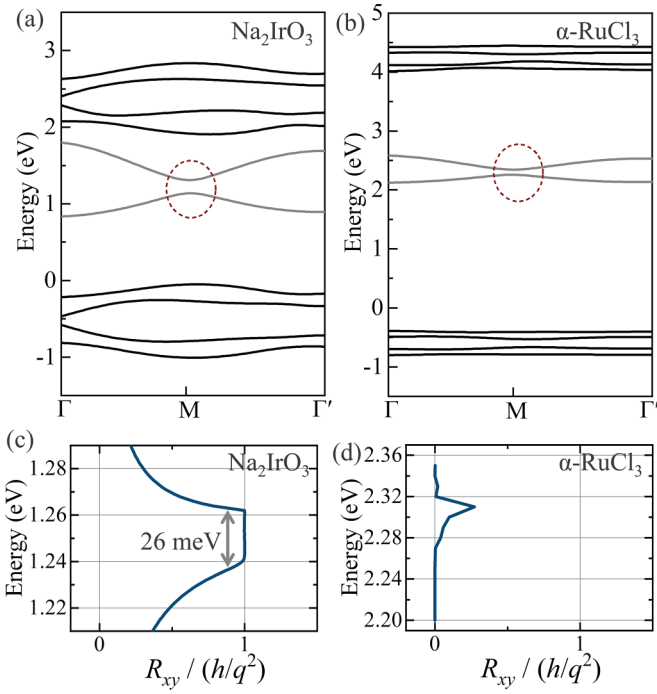

FIG. 5. Band diagram for (a) Na_2IrO_3 and (b) α-$RuCl_3$. Hall resistance is (c) quantized to h/q^2 for Na_2IrO_3 within the gap at the M symmetry point. (d) No quantized Hall effect is observed for α-$RuCl_3$.

Hall conductance due to charge transport in the topological edge state and we do not expect any topological edge conduction in α-$RuCl_3$.

Na_2IrO_3 has been predicted to exhibit a quantum spin Hall (QSH) state at the M symmetry point [27], which is equivalent to a 2D topological insulator with TRS [28] that exhibits a spin-momentum locked linear dispersion. It has been pointed out that Na_2IrO_3 exhibits a persistent energy gap [29,30]. Here, we point out that the energy band in Fig. 5(a) exhibits a small gap at the M symmetry point and an intuitive explanation is that the TRS protected linear dispersion predicted in Ref. [27] should exhibit a gap induced by TRS breaking with a net intrinsic magnetic order along the edge atomic chains. Note that this gap is similar to that observed in magnetic topological insulator [20–23,31]; however, such a gap in Na_2IrO_3 will be induced by the interplay between the isotropic and anisotropic exchange interactions.

Topological phases and QAH state have been theoretically discussed in various ferromagnetic oxides [32–34], and halides [35,36] due to strong SOC. In this Letter, we identify a mechanism for topological edge conduction, which can be observed in specific oxides and halides known for exhibiting strong anisotropic exchange interactions [1,3,15]. We specifically discuss the Hall effect in the 2D channels with zigzag AFM order that will exhibit signatures similar to QAH.

We now show that the topological edge state formation for $K \geqslant 2J$ is a property of the KH model in Eq. (1). For analytical simplicity, we start with a single atomic chain with N lattice points by retaining the zigzag nature of the anisotropic interaction [37,38] as

$$\mathcal{H} = \sum_m \left(J\vec{S}_{m+1} \cdot \vec{S}_m + K^x S^x_{2m} S^x_{2m-1} + K^y S^y_{2m+1} S^y_{2m} \right). \quad (8)$$

We represent the $S = \frac{1}{2}$ spin chains in Eq. (8) using fermionic operators, $|\uparrow\rangle \equiv f^\dagger|\downarrow\rangle$ and $|\downarrow\rangle \equiv f|\uparrow\rangle$ using the Jordan-Wigner transformation [39,40], to get

$$\mathcal{H} = \frac{1}{2}\Big(J + \frac{K}{2} \sum_m (f^\dagger_{m+1} f_m + f^\dagger_m f_{m+1}) - 2J \sum_m n_m - \frac{K}{4} \sum_m (-1)^m (f^\dagger_{m+1} f^\dagger_m + f_m f_{m+1}) + J \sum_m n_{m+1} n_m, \quad (9)$$

where a constant term $N/4$ is ignored. Here, $n_m = f^\dagger_m f_m$ and we assume $K^x = K^y = K$.

We use Fourier transformation around the band minimum $f_m = \frac{1}{\sqrt{N}} \sum_{k'} s_{k'} e^{ik'm}$ to convert Eq. (9) from the real space to the momentum space, as given by

$$\mathcal{H} = \sum_{k'} \left\{ 2J - \frac{2J+K}{2} \cos k' \right\} s^\dagger_{k'} s_{k'} + \sum_{k'} \frac{K}{4} \sin k' (s_{k'} s_{-k'} - s^\dagger_{-k'} s^\dagger_{k'}) + \frac{1}{N} \sum_{k',q} J e^{-iqa} s^\dagger_{k'-q} s^\dagger_{k'} s_{k'-q} s_{k'}, \quad (10)$$

where $k' = k - k_0$. Here, k, q are the wave vector, k_0 is the wave vector at the band minimum, and $s^\dagger_{k'}$ is the creation operator in momentum space. The third term in Eq. (10) represents the interaction term. Here, we consider a case where the atomic chain is a one-dimensional ferromagnet, corresponding to the case for the edge atomic chain for a zigzag AFM order. Under such approximation, the interaction term can be ignored for mathematical simplicity (see, e.g., Ref. [41]) to analyze a first-order dispersion relation.

We transform Eq. (10) into a 2×2 matrix in the particle-hole basis using $\mathcal{H} = \sum_k \Psi^\dagger \mathrm{H} \Psi$ with $\Psi^\dagger \equiv \{s^\dagger_{k'}, s_{-k'}\}$, which yields

$$\mathrm{H} = -J\sigma_z + \frac{2J+K}{4}\sigma_z \cos k' + \frac{K}{4}\sigma_x \sin k'. \quad (11)$$

Equation (11) is in the basis of particle hole; however, here, particle represents an up spin, and the hole represents a down spin. Thus, Eq. (11) has the basis of up and down spins. The energy gap near the band minimum (i.e., $k \to k_0$) is given by $|K - 2J|/2$ [19]. The energy gap near the M symmetry point in Fig. 5(a) for the Na_2IrO_3 case is ∼26 meV, which is very close to the analytical estimation $|K - 2J|/2 \approx 29$ meV. Note that the q^2/h plateau is observed within this energy gap [see Fig. 5(c)] since K and J satisfies the condition $K \geqslant 2J$.

We calculate the topological winding number [42,43] by obtaining the eigenfunction, $\psi(k)$ of Eq. (11), as

$$W_Z = \frac{1}{j\pi} \int_0^{2\pi} dk\ \psi(k)^\dagger \partial_k \psi(k) = \begin{cases} 1; & \text{when } K \geqslant 2J, \\ 0; & \text{when } K < 2J. \end{cases} \quad (12)$$

Here, $W_Z = 0$ for $K < 2J$, indicating a trivial state, while $W_Z = 1$ for $K \geqslant 2J$, indicating topological edge states occurring for a strong anisotropic exchange interaction. Similar one-dimensional arguments for surface state formation in two and three-dimensional topological insulators have been discussed in the past [42]. The analytical conditions obtained from one-dimensional arguments in Eq. (12) exactly correspond to the full tight-binding model-based NEGF results in Fig. 2. Note that the full NEGF calculations consider a general case for the interactions.

In summary, we predict a strong anisotropic exchange interaction induced topological edge conduction in materials with honeycomb lattice structures. The topological edge conductor forms when the strength of the anisotropic interaction exceeds at least twice the strength of the isotropic interaction. For materials like Na_2IrO_3, such strong anisotropic exchange interaction simultaneously induces an intrinsic zigzag antiferromagnetic order that breaks the time-reversal symmetry of the edge conductor. We use a nearest-neighbor tight-binding model and the Kitaev-Heisenberg model to study the quantum transport in such materials and show that the existence of the time-reversal symmetry broken topological edge conductor will be exhibited as a quantized Hall conductance without any external magnetic field.

This work is in part supported by the U.S. Department of Energy, under Contract No. DE-AC02-05-CH11231 within the NEMM program (MSMAG) and in part supported by ASCENT, one of six centers in JUMP, an SRC program sponsored by DARPA.

[1] L. Savary and L. Balents, Quantum spin liquids: A review, Rep. Prog. Phys. **80**, 016502 (2017).
[2] M. Hermanns, I. Kimchi, and J. Knolle, Physics of the Kitaev model: Fractionalization, dynamic correlations, and material connections, Annu. Rev. Condens. Matter Phys. **9**, 17 (2018).
[3] S. M. Winter, A. A. Tsirlin, M. Daghofer, J. van den Brink, Y. Singh, P. Gegenwart, and R. Valentí, Models and materials for generalized Kitaev magnetism, J. Phys.: Condens. Matter **29**, 493002 (2017).
[4] A. Kitaev, Anyons in an exactly solved model and beyond, Ann. Phys. **321**, 2 (2006).
[5] J. Chaloupka, G. Jackeli, and G. Khaliullin, Zigzag magnetic order in the iridium oxide Na_2IrO_3, Phys. Rev. Lett. **110**, 097204 (2013).
[6] F. Ye, S. Chi, H. Cao, B. C. Chakoumakos, J. A. Fernandez-Baca, R. Custelcean, T. F. Qi, O. B. Korneta, and G. Cao, Direct evidence of a zigzag spin-chain structure in the honeycomb lattice: A neutron and x-ray diffraction investigation of single-crystal Na_2IrO_3, Phys. Rev. B **85**, 180403(R) (2012).
[7] R. Schaffer, S. Bhattacharjee, and Y. B. Kim, Quantum phase transition in Heisenberg-Kitaev model, Phys. Rev. B **86**, 224417 (2012).
[8] X. Liu, T. Berlijn, W.-G. Yin, W. Ku, A. Tsvelik, Y.-J. Kim, H. Gretarsson, Y. Singh, P. Gegenwart, and J. P. Hill, Long-range magnetic ordering in Na_2IrO_3, Phys. Rev. B **83**, 220403(R) (2011).
[9] J. A. Sears, M. Songvilay, K. W. Plumb, J. P. Clancy, Y. Qiu, Y. Zhao, D. Parshall, and Y.-J. Kim, Magnetic order in α-$RuCl_3$: A honeycomb-lattice quantum magnet with strong spin-orbit coupling, Phys. Rev. B **91**, 144420 (2015).
[10] R. D. Johnson, S. C. Williams, A. A. Haghighirad, J. Singleton, V. Zapf, P. Manuel, I. I. Mazin, Y. Li, H. O. Jeschke, R. Valentí, and R. Coldea, Monoclinic crystal structure of α-$RuCl_3$ and the zigzag antiferromagnetic ground state, Phys. Rev. B **92**, 235119 (2015).
[11] S.-H. Do, S.-Y. Park, J. Yoshitake, J. Nasu, Y. Motome, Y. S. Kwon, D. T. Adroja, D. J. Voneshen, K. Kim, T.-H. Jang, J.-H. Park, K.-Y. Choi, and S. Ji, Majorana fermions in the Kitaev quantum spin system α-$RuCl_3$, Nat. Phys. **13**, 1079 (2017).
[12] A. Banerjee, J. Yan, J. Knolle, C. A. Bridges, M. B. Stone, M. D. Lumsden, D. G. Mandrus, D. A. Tennant, R. Moessner, and S. E. Nagler, Neutron scattering in the proximate quantum spin liquid α-$RuCl_3$, Science **356**, 1055 (2017).
[13] A. Smith, J. Knolle, D. L. Kovrizhin, J. T. Chalker, and R. Moessner, Majorana spectroscopy of three-dimensional Kitaev spin liquids, Phys. Rev. B **93**, 235146 (2016).
[14] H. Takagi, T. Takayama, G. Jackeli, G. Khaliullin, and S. E. Nagler, Concept and realization of Kitaev quantum spin liquids, Nat. Rev. Phys. **1**, 264 (2019).
[15] S. M. Winter, Y. Li, H. O. Jeschke, and R. Valentí, Challenges in design of Kitaev materials: Magnetic interactions from competing energy scales, Phys. Rev. B **93**, 214431 (2016).
[16] Y. Sizyuk, C. Price, P. Wölfle, and N. B. Perkins, Importance of anisotropic exchange interactions in honeycomb iridates: Minimal model for zigzag antiferromagnetic order in Na_2IrO_3, Phys. Rev. B **90**, 155126 (2014).
[17] J. G. Rau, E. K.-H. Lee, and H.-Y. Kee, Generic spin model for the honeycomb iridates beyond the Kitaev limit, Phys. Rev. Lett. **112**, 077204 (2014).
[18] S. Datta, *Electronic Transport in Mesoscopic Systems* (Cambridge University Press, Cambridge, 1995), p. 377.
[19] See Supplemental Material at http://link.aps.org/supplemental/10.1103/PhysRevB.110.L100407 for the transport modeling parameters and analytical derivations.
[20] C.-Z. Chang, J. Zhang, X. Feng, J. Shen, Z. Zhang, M. Guo, K. Li, Y. Ou, P. Wei, L.-L. Wang, Z.-Q. Ji, Y. Feng, S. Ji, X. Chen, J. Jia, X. Dai, Z. Fang, S.-C. Zhang, K. He, Y. Wang *et al.*, Experimental observation of the quantum anomalous Hall effect in a magnetic topological insulator, Science **340**, 167 (2013).
[21] D. Xiao, J. Jiang, J.-H. Shin, W. Wang, F. Wang, Y.-F. Zhao, C. Liu, W. Wu, M. H. W. Chan, N. Samarth, and C.-Z. Chang, Realization of the axion insulator state in quantum anomalous Hall sandwich heterostructures, Phys. Rev. Lett. **120**, 056801 (2018).
[22] M. Mogi, M. Kawamura, A. Tsukazaki, R. Yoshimi, K. S. Takahashi, M. Kawasaki, and Y. Tokura, Tailoring tricolor structure of magnetic topological insulator for robust axion insulator, Sci. Adv. **3**, eaao1669 (2017).
[23] Y. Deng, Y. Yu, M. Z. Shi, Z. Guo, Z. Xu, J. Wang, X. H. Chen, and Y. Zhang, Quantum anomalous Hall effect in intrinsic magnetic topological insulator $MnBi_2Te_4$, Science **367**, 895 (2020).

[24] S. Hwan Chun, J.-W. Kim, J. Kim, H. Zheng, C. C. Stoumpos, C. D. Malliakas, J. F. Mitchell, K. Mehlawat, Y. Singh, Y. Choi, T. Gog, A. Al-Zein, M. M. Sala, M. Krisch, J. Chaloupka, G. Jackeli, G. Khaliullin, and B. J. Kim, Direct evidence for dominant bond-directional interactions in a honeycomb lattice iridate Na_2IrO_3, Nat. Phys. **11**, 462 (2015).

[25] Y. Kasahara, T. Ohnishi, Y. Mizukami, O. Tanaka, S. Ma, K. Sugii, N. Kurita, H. Tanaka, J. Nasu, Y. Motome, T. Shibauchi, and Y. Matsuda, Majorana quantization and half-integer thermal quantum Hall effect in a Kitaev spin liquid, Nature (London) **559**, 227 (2018).

[26] T. Yokoi, S. Ma, Y. Kasahara, S. Kasahara, T. Shibauchi, N. Kurita, H. Tanaka, J. Nasu, Y. Motome, C. Hickey, S. Trebst, and Y. Matsuda, Half-integer quantized anomalous thermal Hall effect in the Kitaev material candidate α-$RuCl_3$, Science **373**, 568 (2021).

[27] A. Shitade, H. Katsura, J. Kuneš, X.-L. Qi, S.-C. Zhang, and N. Nagaosa, Quantum spin Hall effect in a transition metal oxide Na_2IrO_3, Phys. Rev. Lett. **102**, 256403 (2009).

[28] M. König, S. Wiedmann, C. Brüne, A. Roth, H. Buhmann, L. W. Molenkamp, X.-L. Qi, and S.-C. Zhang, Quantum spin Hall insulator state in HgTe quantum wells, Science **318**, 766 (2007).

[29] N. Alidoust, C. Liu, S.-Y. Xu, I. Belopolski, T. Qi, M. Zeng, D. S. Sanchez, H. Zheng, G. Bian, M. Neupane, Y.-T. Liu, S. D. Wilson, H. Lin, A. Bansil, G. Cao, and M. Z. Hasan, Observation of metallic surface states in the strongly correlated Kitaev-Heisenberg candidate Na_2IrO_3, Phys. Rev. B **93**, 245132 (2016).

[30] F. Lüpke, S. Manni, S. C. Erwin, I. I. Mazin, P. Gegenwart, and M. Wenderoth, Highly unconventional surface reconstruction of Na_2IrO_3 with persistent energy gap, Phys. Rev. B **91**, 041405 (2015).

[31] C. Liu, Y. Wang, H. Li, Y. Wu, Y. Li, J. Li, K. He, Y. Xu, J. Zhang, and Y. Wang, Robust axion insulator and chern insulator phases in a two-dimensional antiferromagnetic topological insulator, Nat. Mater. **19**, 522 (2020).

[32] L. Si, O. Janson, G. Li, Z. Zhong, Z. Liao, G. Koster, and K. Held, Quantum anomalous Hall state in ferromagnetic $SrRuO_3$ (111) bilayers, Phys. Rev. Lett. **119**, 026402 (2017).

[33] H. P. Wang, W. Luo, and H. J. Xiang, Prediction of high-temperature quantum anomalous Hall effect in two-dimensional transition-metal oxides, Phys. Rev. B **95**, 125430 (2017).

[34] S.-J. Zhang, C.-W. Zhang, S. Zhang, W.-X. Ji, P. Li, P.-J. Wang, S.-S. Li, and S.-S. Yan, Intrinsic Dirac half-metal and quantum anomalous Hall phase in a hexagonal metal-oxide lattice, Phys. Rev. B **96**, 205433 (2017).

[35] X.-L. Sheng and B. K. Nikolić, Monolayer of the 5*d* transition metal trichloride $OsCl_3$: A playground for two-dimensional magnetism, room-temperature quantum anomalous Hall effect, and topological phase transitions, Phys. Rev. B **95**, 201402 (2017).

[36] C. Huang, J. Zhou, H. Wu, K. Deng, P. Jena, and E. Kan, Quantum anomalous Hall effect in ferromagnetic transition metal halides, Phys. Rev. B **95**, 045113 (2017).

[37] C. E. Agrapidis, J. van den Brink, and S. Nishimoto, Ordered states in the Kitaev-Heisenberg model: From 1d chains to 2d honeycomb, Sci. Rep. **8**, 1815 (2018).

[38] E. Sela, H.-C. Jiang, M. H. Gerlach, and S. Trebst, Order-by-disorder and spin-orbital liquids in a distorted Heisenberg-Kitaev model, Phys. Rev. B **90**, 035113 (2014).

[39] G. Kells, J. K. Slingerland, and J. Vala, Description of Kitaev's honeycomb model with toric-code stabilizers, Phys. Rev. B **80**, 125415 (2009).

[40] A. A. Zvyagin, Generalizations of exactly solvable quantum spin models, Phys. Rev. B **101**, 094403 (2020).

[41] P. Coleman, Simple examples of second quantization, in *Introduction to Many-Body Physics* (Cambridge University Press, Cambridge, 2015), p. 71–94.

[42] S. S. Pershoguba and V. M. Yakovenko, Shockley model description of surface states in topological insulators, Phys. Rev. B **86**, 075304 (2012).

[43] R. S. K. Mong and V. Shivamoggi, Edge states and the bulk-boundary correspondence in Dirac Hamiltonians, Phys. Rev. B **83**, 125109 (2011).